Computation of Nonequilibrium Merged Stagnation Shock Layers by Successive Accelerated Replacement

THOMAS C. DELLINGER*
General Electric Company, Philadelphia, Pa.

Results are presented for fully merged shock layer computations in the stagnation region of a hypersonic body. Numerical solutions are obtained with a new technique which avoids several troublesome aspects of previous methods. The effects of nonequilibrium chemistry are studied for a multicomponent air mixture and the resulting electron concentrations are calculated. The analysis assumes a continuum approach and employs the well known "locally similar" flow model. The governing system of equations constitutes a two-point boundary value problem which is solved using a simple finite difference method called successive accelerated replacement, or SAR. Special attention is given to a singularity that appears in the continuity equation, and the importance of an acceleration factor on the convergence of the solution is discussed. Solutions are obtained for a Reynolds number range of 814 to 4000 and for flight speeds from 15,000 to 26,000/fps. Predicted results for the electron concentration are compared with experimental data and good agreement is obtained.

Nomenclature

C_i = mass fraction of species i
E = function defined in Eq. (14)
h = static enthalpy, $\bar{h}/\bar{H}_\infty$
h_i = static enthalpy of species i, $\bar{h}_i/\bar{H}_\infty$
H = total enthalpy, $\bar{H}/\bar{H}_\infty$
Le = Lewis number
$\bar{M}_i$ = molecular weight of species i
M = mixture molecular weight, defined in Eq. (7)
MP = number of mesh points
n = coordinate normal to body surface, $\bar{n}/\bar{R}_N$
N = Nth mesh point
NS = number of chemical species
p = pressure, $\bar{p}/\bar{\rho}_\infty \bar{V}_\infty^2$
p_2 = auxiliary pressure, $\bar{p}_2/\bar{\rho}_\infty \bar{V}_\infty^2$
Pr = Prandtl number
$\bar{R}_0$ = universal gas constant
$\bar{R}_N$ = stagnation point nose radius
Re = Reynolds number, $\bar{\rho}_\infty \bar{V}_\infty \bar{R}_N/\bar{\mu}_\infty$
s = coordinate parallel to body surface, $\bar{s}/\bar{R}_N$
T = temperature, $\bar{T}/\bar{T}_\infty$
u = s velocity, $\bar{u}/\bar{V}_\infty$
u_1 = velocity gradient, $(d\bar{u}/d\bar{s})(\bar{R}_N/\bar{V}_\infty)$
U = function defined in Eq. (12)
v = n velocity, $\bar{v}/\bar{V}_\infty$
V = function defined in Eq. (13)
$\bar{V}_\infty$ = freestream velocity
$\bar{w}_i$ = chemical source term of species i
X_i = function defined in Eq. (11)
Δ = mesh spacing
ϵ = convergence constant
η = transformed normal coordinate, n/n_e
μ = viscosity, $\bar{\mu}/\bar{\mu}_\infty$
ρ = density, $\bar{\rho}/\bar{\rho}_\infty$
σ = convergence factor
ω = acceleration factor

Subscripts

w = wall conditions
e = edge or effective freestream
∞ = freestream conditions

Superscripts

$'$ = derivative with respect to η
$-$ = dimensional quantity

Presented as Paper 69-655 at the AIAA Fluid and Plasma Dynamics Conference, San Francisco, Calif., June 16-18, 1969; submitted June 18, 1969; revision received June 29, 1970.

* Engineer, Re-Entry and Environmental Systems Division, Fluid Mechanics and Chemistry Laboratory. Associate Member AIAA.

I. Introduction

MANY effects arising from the interaction of an electromagnetic signal and a re-entry vehicle depend upon the level of ionization occurring in the stagnation region shock layer. For flight in rarefied atmospheres, an accurate prediction of this ionization requires an analysis which correctly models the flowfield structure and which accounts for the effects of finite rate chemistry. The flow regimes encountered for various rarefied flight conditions are discussed in Ref. 1. This paper considers the merged layer regime, a continuum but rarefied flow situation in which viscous effects are important in the entire region between the body surface and the freestream. An analysis is developed which permits the direct computation of the ionization in a merged stagnation shock layer for a chemical nonequilibrium, multicomponent gas mixture. The numerical solutions are obtained using a finite difference technique called successive accelerated replacement, or simply, SAR. This method not only allows the coupled calculation of the ionization and the detailed flow structure, but also avoids several troublesome aspects of numerical methods previously used in merged layer analyses.

There have been many previous investigations[2-8] of rarefied stagnation shock layers. Unfortunately, most of the analyses were developed for a perfect gas, and are not directly applicable to the problem of predicting the flowfield ionization. Recently, however, chemical relaxation effects were treated by Chung et al.,[9] who obtained nonequilibrium merged stagnation solutions for a binary dissociating gas. In addition, using an approximate model, Lee and Zierten[10] have made calculations for nonequilibrium merged layer ionization. In their model, they solve the species conservation equations for a multicomponent gas mixture, but use neutral gas flow properties which are assumed a priori. In their applications, these properties are given by frozen flow solutions obtained according to the method of Chung et al.[9] Thus, the model is valid whenever the neutral gas properties are accurately represented by their frozen flow values and are not appreciably affected by either the presence of ionization or any chemical reactions. Otherwise, an analysis is required which uses a realistic gas model and which

simultaneously calculates the ionization and the neutral gas flow field.

Such an analysis is developed in the present work. For the cases investigated, the results tend to show that an uncoupled calculation for the ionization, such as Lee and Zierten's,[10] may not always be satisfactory. Moreover, with the present method, solutions are obtained for high Reynolds number cases where the method of Chung et al.[9] experiences numerical difficulties. Predicted results for electron concentration have been compared with experiment and good agreement is obtained.

The problem is formulated in Sec. II, which includes the approach, the governing equations and the gas model. Section III gives the details of the present numerical scheme and lists some of its advantages. In addition, problems concerning the stability and convergence of the method and a singularity in the continuity equation are discussed. In Sec. IV, the results of the numerical computations are presented and comparisons are made with experimental data and other theoretical predictions. The major conclusions are summarized in Sec. V.

II. Formulation of the Problem

A. Approach

This investigation considers the stagnation merged layer flow of a chemical nonequilibrium, multicomponent gas mixture. The flow geometry, which is shown in Fig. 1, extends along the stagnation streamline from the body surface to the undisturbed freestream. The analysis assumes a continuum flow, a thin shock layer and the well-known locally similar stagnation flow model. Questions regarding the validity of the continuum approach and the details of the derivation of the simplified Navier-Stokes, energy and species equations have been considered elsewhere[7-9,11] and are not treated here.

B. Governing Equations

When the gas is chemically inert, the equations used in this analysis are exactly those used by Chung et al.[9]; hence, for frozen flow, the results of the present technique can be checked against the results given in Ref. 9. In order to make the nonequilibrium calculations, the species conservation equations and appropriate expressions for the mixture enthalpy and molecular weight are added to the system. The only diffusion allowed is that due to species gradients; however,

Table 1 Reaction system

	Reaction
No. = 1	$O_2 + M \rightleftarrows O + O + M$
2	$N_2 + M \rightleftarrows N + N + M$
3	$NO + M \rightleftarrows N + O + M$
4	$NO + O \rightleftarrows O_2 + N$
5	$N_2 + O \rightleftarrows NO + N$
6	$N + O \rightleftarrows NO^+ + e^-$

Reaction rate constants,[a] $k_{f,r} = A_{f,r}T^{B_{f,r}} \exp(-C_{f,r}/RT)$

No.	A_f	A_r	B_f	B_r	C_f	C_r
1	2.5×10^{16}	8.9×10^{14}	−0.5	−0.44	117945	0
2	2.0×10^{21}	1.91×10^{20}	−1.5	−1.57	225014	0
3	5.5×10^{20}	1.67×10^{20}	−1.5	−1.52	150002	0
4	3.2×10^{9}	2.67×10^{20}	1.0	0.92	39100	7042.5
5	6.8×10^{13}	2.13×10^{13}	0	−0.04	75011.5	0
6	6.4×10^{9}	7.0×10^{18}	0.5	−0.90	63356.5	0

Third body efficiencies (based on argon = 1)

No.	O_2	N_2	N	O	NO
1	5	2	2	25	2
2	2	5	3	5	2
3	2	2	5	5	2

[a] Units: moles/cm³, sec, °K, cal/mole.

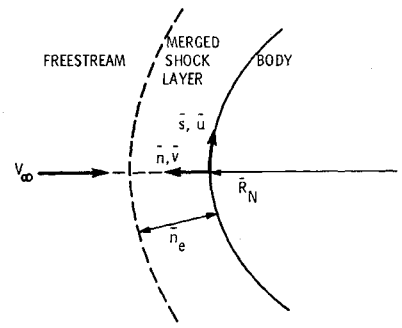

Fig. 1 Coordinate system and flow geometry.

multicomponent diffusion is neglected and all species have been assigned a constant value of $Le = 1$. This also serves to simplify the energy equation.

For axisymmetric flow and in terms of the transformed normal coordinate, $\eta = n/n_e$, the dimensionless equations for $Pr = \frac{3}{4}$ are as follows:

$$\rho'/\rho = -[2n_e(u_1 + v) + v']/v \tag{1}$$

$$\mu C_i'' + (\mu' - 3n_eRe\rho v/4)C_i' + 3n_e^2Re\rho\bar{w}_iR_N/4V_\infty = 0 \quad i = 1,2,\ldots,NS \tag{2}$$

$$\mu u_1'' + (\mu' - n_eRe\rho v)u_1' - n_e^2Re\rho[u_1^2 + u_1v - (2p + p_2)/\rho] = 0 \tag{3}$$

$$\mu v'' + (\mu' - 3n_eRe\rho v/4)v' - 3n_eRep'/4 + n_e(\mu u_1' - 2u_1\mu')/2 = 0 \tag{4}$$

$$p_2' = -2n_e\rho u_1(u_1 + v) \tag{5}$$

$$\mu H'' + (\mu' - 3n_eRe\rho v/4)H' = 0 \tag{6}$$

$$p = \bar{R}_0\bar{T}_\infty\rho T/\bar{V}_\infty^2\bar{M}_\infty M \tag{7}$$

$$M = 1/\sum_i \bar{M}_\infty(C_i/\bar{M}_i)$$

$$\mu = 1.229T^{0.625} \tag{8}$$

$$H = h + \bar{V}_\infty^2v^2/2\bar{H}_\infty,\ h = \sum_i C_ih_i \tag{9}$$

There are $6 + NS$ equations for the solution of the $6 + NS$ unknowns u_1,v,ρ,p,T,p_2 and $C_i,i = 1,2,\ldots NS$. The number of required boundary conditions for Eqs. (1–7) is equal to $8 + 2\ NS$. The boundary conditions used in this analysis are

$$\begin{aligned} \eta = 0: &\quad v = 0,\ T = Tw,\ C_i = C_{iw} \\ \eta = 1: &\quad v = -1,\ \rho = 1, \\ &H = 1,\ p_2 = -2p_\infty,\ C_i = C_{i\infty} \end{aligned} \tag{10}$$

These boundary conditions are split with the location of the outer boundary (freestream) initially unknown.

C. Gas Model

The nonequilibrium calculations are made for a seven-species, six-reaction air model. The species are O_2, N_2, N, O, NO, NO^+ and e^-. The appropriate chemical reactions for the conditions of interest in this work and the expressions used to evaluate the corresponding forward and reverse reaction rate constants are listed in Table 1. Electron concentrations are calculated assuming charge neutrality. A fully catalytic wall boundary condition is used for all the cases investigated so that at the wall the mass fractions of the dissociation and ionization products (O, N, NO and NO^+) are zero and the molecular species (O_2, N_2) assume their undissociated freestream values.

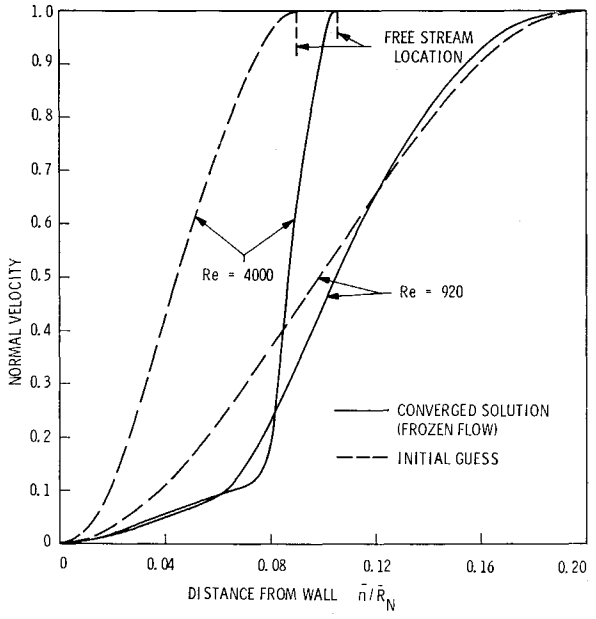

Fig. 2 Profiles of initial guesses and converged solutions for normal velocity at Re = 920, 4000.

For nonequilibrium flow, the species enthalpy, h_i, is obtained from curve fit formulas of the appropriate thermodynamic calculations for the temperature ranges $\bar{T} \leq 300°K$, $300 < \bar{T} < 1600°K$, $1600 \leq \bar{T} < 6000°K$, $6000 \leq \bar{T} < 20{,}000\ °K$ and $\bar{T} \geq 20{,}000°K$. For frozen flow, the static enthalpy is calculated according to Ref. 9 as $h = 9\bar{R}_0\bar{T}_\infty T/2\bar{M}_\infty\bar{H}_\infty$.

III. Method of Solution

A. Choice of a Method

Equations (1–7) constitute a set of coupled nonlinear first- and second-order ordinary differential equations with split boundary conditions and with one boundary location initially unknown. Previous solutions have been reported only for a perfect gas or a simplified real gas approximation to these equations. The solutions have been obtained by either the so-called shooting or ballistic[4,5] integration schemes or by finite difference techniques.[12,13] In the shooting methods, iteration must be performed on a number of unknown initial conditions until the proper boundary values are obtained at the other end of the range of integration. The task of specifying a consistent set of these unknown conditions can become prohibitively difficult, especially when the required number is large as is the case for systems with complex chemistry. In addition, the shooting method becomes difficult to apply when the boundary conditions to be matched are specified at $n \to \infty$ as in the present merged layer case. In the finite difference schemes, either an approximate set of linear[12] difference equations or the fully coupled nonlinear[13] difference equations are solved. The former method suffers from the difficulty of obtaining a stable set of difference approximations whereas both methods require very accurate initial guesses throughout the entire range of integration in order to obtain convergence.

In this analysis, a remarkably simple and rapid numerical finite difference method, SAR, is employed for the solution of the governing equations. This method is used because of its previously successful application to boundary layer problems[14,15], but, mainly, because it avoids the difficulties mentioned previously for the alternative methods.

As applied in this problem, the SAR method possesses the following advantages: 1) All boundary conditions are satisfied exactly at each stage of the calculation; 2) The difference approximations are simple and straightforward and unequal mesh sizes are not necessary; 3) An exact solution to the fully nonlinear difference equations is obtained without need to allow for the complete coupling between the equations; 4) The ability to obtain a converged solution does not critically depend on the accuracy of the initial guesses. Moreover, the SAR method is used only for the second-order equations while those of first-order are handled in the usual fashion of initial value problems.

B. Successive Accelerated Replacement

SAR is applied to Eqs. (2–4, and 6), which are written as

$$X_i(C_i'',C_i';\mu',\rho,v,\mu,\bar{w}_i,n_e) = 0 \tag{11}$$

$$U(u_1'',u_1',\mu',u_1,v,\rho,p,\mu,p_2,n_e) = 0 \tag{12}$$

$$V(v'',v',p',\mu',u_1,v,\rho,\mu,n_e) = 0 \tag{13}$$

$$E(H'',H',\mu',v,\rho,\mu,n_e) = 0 \tag{14}$$

Solutions are desired for the region $0 < \eta < 1$, which is divided into MP equal intervals of length $\Delta = 1/MP$. Equations (11–14) are then replaced by their finite difference approximations. For the first and second derivatives

$$Z_N' = (Z_{N+1} - Z_{N-1})/2\Delta,$$
$$Z_N'' = (Z_{N+1} + Z_{N-1} - 2Z_N)/\Delta^2 \tag{15}$$

respectively, where Z_N is the value of any one of the variables C_i,u_1,v,H or μ at the Nth mesh point. Next, initial guesses are made for all of the flow variables at each mesh point. In the general scheme, each of the unknowns C_i,u_1,v, or H is matched with a particular equation from the set, Eqs. (11–14). This equation alone is used to generate corrections to the given variable. The general effect of this procedure is to uncouple the system of equations. In this work, Eq. (11) is matched with C_i, Eq. (12) with u_1, Eq. (13) with v, and Eq. (14) with H. Corrections to the initial guesses are calculated for each of the variables using formulas exactly similar to the one illustrated below for the variable v.

The $k+1$ approximation to the variable v at the Nth point in the profile is calculated from

$$v_N{}^{k+1} = v_N{}^k - \omega_v V_N/(dV_N/dv_N) \tag{16}$$

It has been sufficient in this work to use $dV_N/dv_N = -2/\Delta^2$, which follows from the differentiation of the finite difference approximation for the second derivative term in Eq. (13). The same procedure is followed for the terms dX_i/dC_i, dU/du_1, and dE/dH. The acceleration factors ω_{C_i}, ω_{u_1}, ω_v, and ω_H are chosen to control the convergence of the solution and will be discussed in a later section. New values of C_i, u_1, v, and H are calculated for each mesh point, starting with the first point away from the wall ($N = 2$) and proceeding to the first point away from the freestream ($N = MP$). The scheme is one of successive replacement in the sense that new values are used as soon as they are available.

The remaining variables are calculated as follows. For given values of H, v, and C_i, Eq. (9) is used to determine the temperature. Knowing the temperature, the viscosity is then calculated. When new values for u_1 and v have been determined for the entire profile, the density and the pressure term p_2 are calculated by numerical quadrature from the freestream to the body using Eqs. (1) and (5), respectively. Pressure is then determined from the equation of state.

C. Freestream Location

Provided that the correct value of n_e has been used, the procedure given previously can be iterated to obtain the desired solution. However, if the value which is specified for the freestream location is too small, the solution will not have the

proper asymptotic behavior at the outer edge; that is, some or all of the properties will have nonvanishing first derivatives. On the other hand, difficulties can arise in maintaining a stable calculation in the constant property freestream region when the value assumed for n_e is larger than the value actually needed. In the present scheme, the correct location of the freestream is determined as an integral part of the over-all calculation. Using the fact that the temperature is one of the first properties to feel the impending shock transition, the value of n_e is adjusted in order to satisfy the requirement that the first derivative of the temperature be less than a prescribed small value. The freestream locations determined in this fashion have always been associated with a solution in which all of the other flow properties possess the correct asymptotic form.

D. Initial Guesses and Convergence

Previous investigations of this problem using finite differences have found that accurate initial guesses are needed in order to obtain converged solutions. Fortunately, this problem was not experienced with the SAR method as employed in this work. Here, initial values are obtained using simple polynomial expressions for the properties u_1, v, and H and constant values for p_2 and the species mass fractions. Using these initial values and a guess for n_e, the remaining flow properties T, μ, ρ, and p can be determined. In general, the guesses are used to obtain the frozen flow results, which then are used along with the mass fraction guesses as the initial values for the corresponding nonequilibrium calculations.

The successful application of the present method does not critically depend on how well the initial guesses approximate the converged solution. Figure 2 shows that accurate initial guesses are not needed in order to obtain a converged solution with the present method. Profiles are shown for the initial guesses and for the converged solutions of normal velocity for two widely different Reynolds numbers. The results shown in Fig. 2 for the normal velocity are typical of the large differences between the initial and converged values of the other variables as well. However, in the present scheme, the development of the solution depends quite strongly on the initial guess for the normal velocity.

Using the guessed values of u_1, v, and n_e, Eq. (1) can be integrated to give the density profile. It turns out, however, that the density obtained in this manner is very sensitive to the value of v since $\rho'/\rho \sim v'/v$. This is especially true near the wall where $v \to 0$. Unless the normal velocity profile (and to a much lesser extent, the u_1 profile) is very accurate near the wall, the density and, hence, the pressure will be very poor approximations to their correct values. The effect of this inaccurate pressure shows up primarily in the subsequent calculations for the corrections to the normal velocity. These calculations are made using Eqs. (13) and (16). It happens that near the wall, Eq. (13) depends primarily on the term $3n_eRep'/4\mu$ and the incorrect pressure results in a large correction to v as calculated from Eq. (16). Thus, there is a strong coupling between the density calculated using Eq. (1) and the normal velocity calculated using Eq. (13). Of course, the entire set of equations is coupled, and the remaining equations will be influenced as well. This coupling must be reduced or controlled or else the present solution scheme will diverge rapidly.

It has been found that a stable calculation can be maintained by a proper choice of the value of the acceleration factors. The present scheme for determining the acceleration factors is illustrated below for the variable v. The other acceleration factors are determined by an identical procedure.

First, it is required that

$$|(v_N{}^{k+1} - v_N{}^k)/v_N{}^k| = \omega_v|V_N\Delta^2/2v_N{}^k| < \epsilon \qquad (17)$$

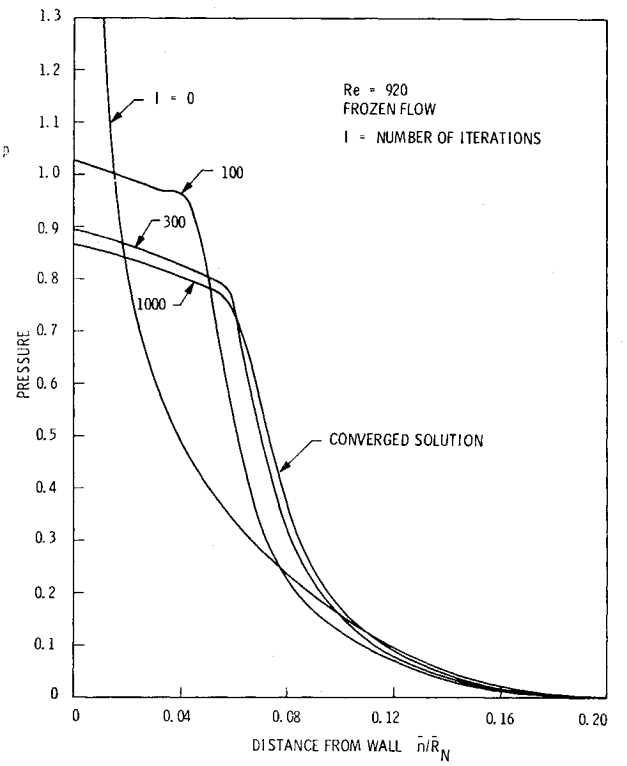

Fig. 3 Typical relaxation of the pressure profile from initial values to converged solution.

from which we define

$$\sigma_v = \epsilon|2v_N{}^k/\Delta^2V_N| \qquad (18)$$

Then, whenever $\sigma_v < 1$, we set $\omega_v = \sigma_v$, and if $\sigma_v \geq 1$, we set $\omega_v = 1$. A value of $\epsilon = 0.01$ has been used successfully in all of the cases investigated in this work. Some typical results using this scheme are shown for the pressure in Fig. 3. The initial pressure is seen to be a very poor approximation to the converged value. Using a constant acceleration factor of unity would have resulted in an almost immediate divergence of the solution for this case. Considering the quality of the initial guesses, the convergence of the solution is quite rapid. After 1000 iterations the pressure was only changing in the fifth significant digit, and the entire solution required only approximately two minutes on the GE 635 computer.

The finite difference mesh size can also have an effect on the convergence of the solution; however, its effect was not studied extensively in this work. Instead, a value of $\Delta \approx 0.02$, corresponding to approximately fifty mesh points, has been used successfully for all the cases investigated so far. The advantage of using a larger mesh spacing is the reduction in computer time, but since lengthy computer times were not a problem here, no effort was made to establish the maximum allowable increment for a given case.

E. Singularity in the Continuity Equation

Examination of Eq. (1) shows that there is a singularity in the continuity equation where the normal velocity vanishes. In this work this point occurs at the wall because of the boundary condition $v_w = 0$. This presents a difficulty in the numerical integration of Eq. (1) to obtain the density. Since the singularity does not permit a value for $(\rho'/\rho)_w$ to be calculated, the integration cannot be carried all the way to the wall. As a result, the integration does not yield a value for the wall density, or equivalently, the wall pressure which is the quantity actually required in the calculations (see Eq. (4)). However, even if a value for $(\rho'/\rho)_w$ were

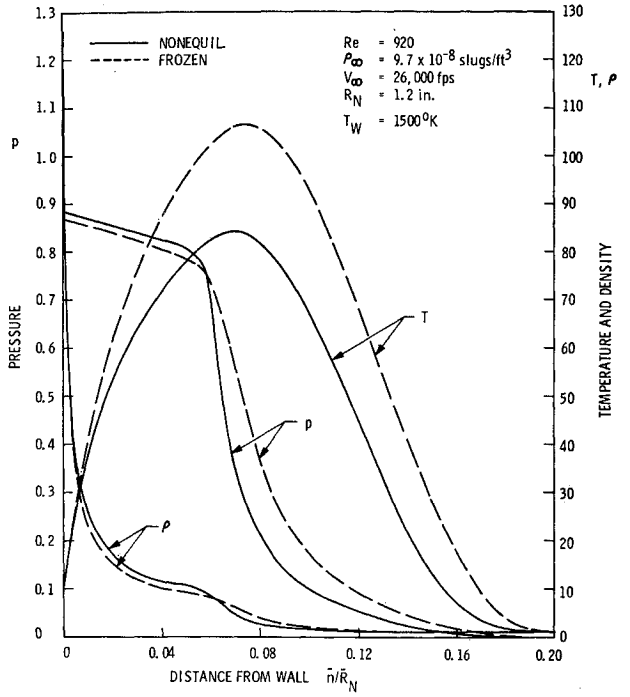

Fig. 4 Temperature, pressure, and density profiles at *Re* = 920 for frozen and nonequilibrium flow.

available, the present results indicate that the density has a very steep slope near the wall and requires a small step size in order to perform the integration accurately in that region.

An alternative method is employed to predict the wall pressure in the present work. The density is obtained in the usual fashion by integrating Eq. (1). However, the integration is only carried as far as the first point away from the wall. The corresponding pressures are obtained from the equation of state. The final pressure is obtained from the linear expression

$$p_w = p_\Delta - \Delta p_w' \tag{19}$$

which satisfies the conditions $p = p_\Delta$ at $\eta = \Delta$ and $p' = p_w'$ at $\eta = 0$. The relation for p_w' is derived from Eq. (4) and is

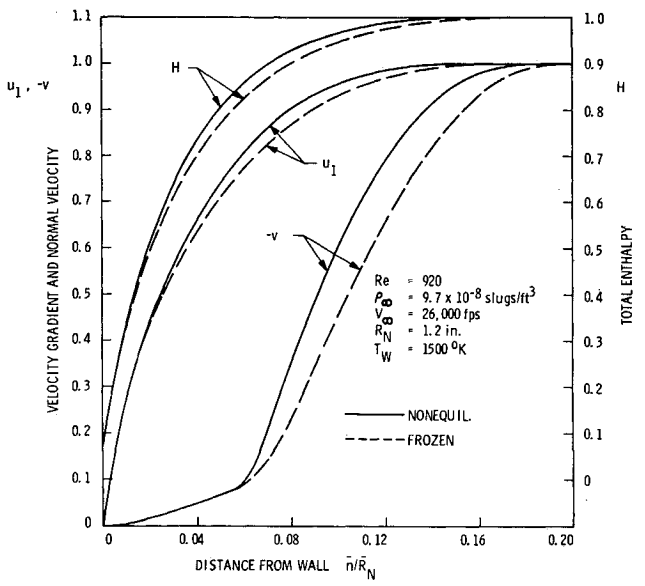

Fig. 5 Velocity gradient, normal velocity, and total enthalpy profiles at *Re* = 920 for frozen and nonequilibrium flow.

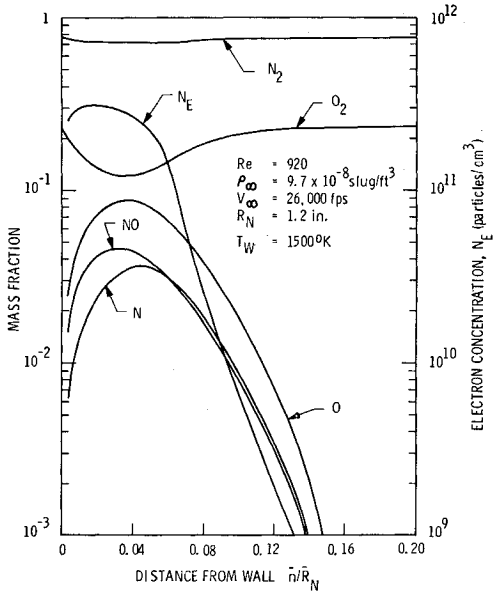

Fig. 6 Species mass fraction and electron concentration profiles for *Re* = 920.

given by

$$p_w' = (4/3n_eRe)[\mu v'' + \mu' v' + (n_e \mu u_1'/2)]_w \tag{20}$$

The finite difference approximations for the derivatives are

$$v_w'' \simeq v_2'' = (v_3 - 2v_2)/\Delta^2,\ v_w' = (4v_2 - v_3)/2\Delta$$
$$u_{1,w}' = (4u_{1,2} - u_{1,3})/2\Delta \tag{21}$$

where $v = v_2$ at $\eta = \Delta$, $v = v_3$ at $\eta = 2\Delta$, etc., and where the conditions $v_w = 0$ and $u_{1,w} = 0$ have been used in Eqs. (20) and (21). It should be noted that in the converged solutions $v_w' = 0$, which is the constraint required in Eq. (1) in order to have a finite density at the wall. The main utility of this approach is that it avoids the difficulties associated with integrating Eq. (1) in a region where the density is varying rapidly.

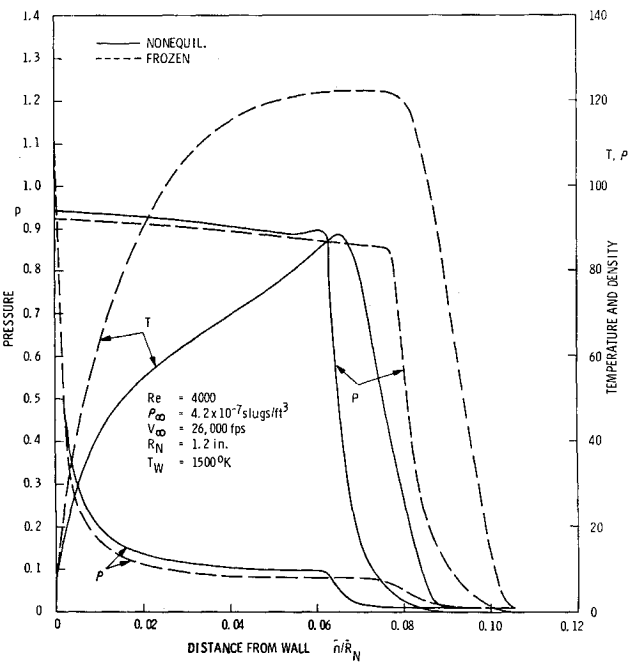

Fig. 7 Temperature, pressure, and density profiles at *Re* = 4000 for frozen and nonequilibrium flow.

IV. Results

As a check on the present method, a frozen flow calculation was made corresponding to a case considered by Chung et al.[9] For this case, $Re = 920$, $\bar{V}_\infty = 26{,}000$ fps, and $\bar{T}_W = 1500°$K. Nonequilibrium calculations were also made at these conditions for a fully catalytic wall, a single nose radius, $\bar{R}_N = 1.2$ in., and at the additional Reynolds number of 4000. The densities at $Re = 920$ and 4000 are 9.7×10^{-8} and 4.2×10^{-7} slugs/ft^3, corresponding to altitudes of approximately 240,000 and 204,000 ft, respectively. Two other calculations were performed to compare the present electron concentrations with experimental data and other theoretical predictions. Comparisons are made with the theoretical results of Lee and Zierten[10] for a case with $Re = 814$, $\bar{V}_\infty = 23{,}000$ fps, $\bar{T}_W = 1500°$K, $\bar{R}_N = 0.675$ in., and $\bar{\rho}_\infty = 1.72 \times 10^{-7}$ slugs/ft^3. A comparison with experiment is made for the test results given in Ref. 16 for the conditions: $Re = 3160$, $\bar{V}_\infty = 15{,}000$ fps, $\bar{T}_W = 300°$K, $\bar{R}_N = 3$ in., and $\bar{\rho}_\infty = 3.49 \times 10^{-7}$ slugs/ft^3.

Figures 4–8 present the frozen and nonequilibrium results for $Re = 920$ and 4000. The frozen flow properties shown in Figs. 4 and 5 correspond to a case considered by Chung et al.[9] Practically no difference was found between the present frozen flow results and the results given in Ref. 9, which were, of course, obtained using a different numerical method. The frozen and nonequilibrium flow properties are compared in Figs. 4, 5, and 7. As the Reynolds number is increased, the frozen flow approximation becomes worse throughout the merged layer. However, the largest differences in the flow properties occur in the shock transition region, which moves closer to the body at a faster rate for a nonequilibrium flow than for a frozen flow. The results also show the development of the bow shock wave as it becomes thinner with increasing Reynolds number. A good estimate of the extent of the shock transition region can be made by measuring its thickness relative to the location of the peak temperature point. As the Reynolds number is increased from 920 to 4000, the nonequilibrium results show that this thickness decreases from approximately 70% to 25% of the total merged layer thickness. At the same time, however, the merged layer thickness is more than halved, but yet the location of the peak temperature point remains practically unchanged. The over-all result is a shock thickness five times as small at $Re = 4000$ than at $Re = 920$.

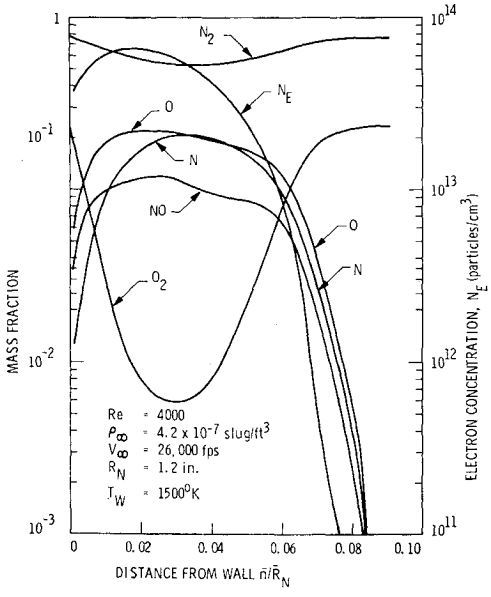

Fig. 8 Species mass fraction and electron concentration profiles for $Re = 4000$.

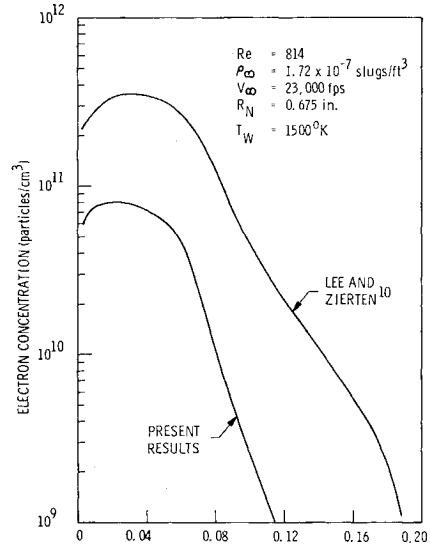

Fig. 9 Comparison with the theoretical results of Lee and Zierten[10] for electron concentration.

The reduced merged layer thickness for the nonequilibrium flows is a result of the increased density due to the dissociation. The mass fraction and electron concentration profiles for $Re = 920$ and 4000 are shown in Figs. 6 and 8, respectively. These figures show the large increase in dissociation with an increase in the Reynolds number, which is equivalent in this case to an increase in the freestream density. At $Re = 4000$, the mass fraction of molecular oxygen is more than an order of magnitude lower than at $Re = 920$. A similar but smaller increase in dissociation is noted for nitrogen. It is noted that the peak dissociation occurs closer to the body than the location of the peak temperature point. This is due in part to the fact that the maximum temperature occurs within the density transition region where the density is still increasing, and also to the fact that just downstream of the temperature maximum, the atom concentrations are increasing rapidly and the shuffle reactions 4 and 5 (see Table 1) become more important.

An even larger effect is noted for the electron concentration. The peak values differ by more than two orders of magnitude over this Reynolds number range.

In order to make a theoretical comparison, results have been obtained for a case considered by Lee and Zierten.[10] The electron concentrations are shown in Fig. 9. The results of the present analysis were obtained using the reaction rates given in Table 1; however, in order to make a comparison as identical as possible, a calculation was also made using the same reaction rates employed by Lee and Zierten. Practically no difference was found between the predictions for electron concentration using the two sets of reaction rates. In particular, the results using Lee and Zierten's rates were lower than the present results, the difference being less than 10% throughout the merged layer. From Fig. 9, it is seen that the present results for electron concentration are lower by a factor of about four at the peak values and even lower elsewhere. A possible explanation for this result can be found by examining the corresponding flowfield properties given in Fig. 10. There, the results of frozen and nonequilibrium calculations using the present technique are compared with the nonequilibrium results for temperature taken from Ref. 10. It is noted that throughout most of the shock transition region, the temperatures of Lee and Zierten are on the average about 2000°K higher than the present nonequilibrium results. The higher temperature is believed responsible for the observed differences in the electron con-

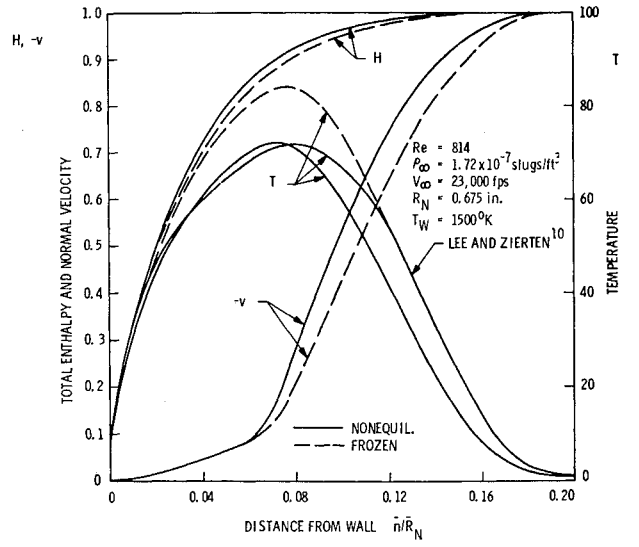

Fig. 10 Total enthalpy, temperature, and normal velocity profiles at *Re* = 814 for frozen and nonequilibrium flow.

centrations, because of its effect on the chemical reaction rates and the increased chemical activity.

This effect is shown in Fig. 11, which compares the chemical production rates resulting from the two analyses when the same reaction rates are used. It is seen that the higher temperatures lead to an increased dissociation of oxygen and nitrogen and, hence, to a larger production of electrons by the associative ionization reaction giving NO^+.

In order to explain the temperature difference, it is necessary to review briefly the method of Lee and Zierten. In their analysis, the species concentrations and the corresponding values of temperature and density are calculated using given values of the pressure, normal velocity and static enthalpy. As discussed previously, the properties which are assumed known are taken from frozen flow solutions calculated according to the method of Chung et al.[9] For purposes of this argument, it has been assumed that the present frozen flow results accurately represent those used in Ref. 10.

Figure 10 shows that while there is a small difference between the frozen and nonequilibrium values of total enthalpy, there is a relatively large difference between the normal velocities and, hence, between the static enthalpies. It should be noted that for a given total enthalpy, a given percent change in the normal velocity results in an even larger percent

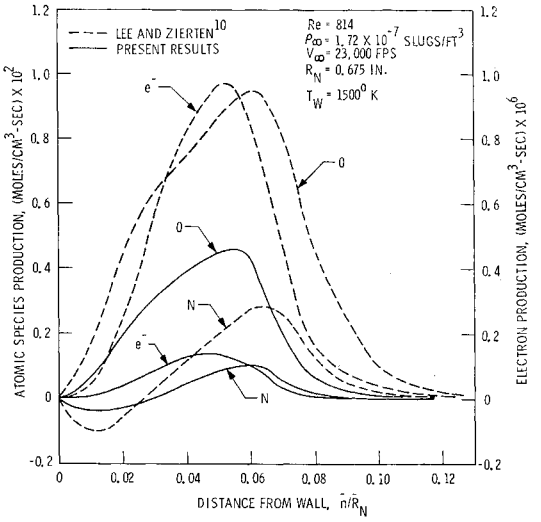

Fig. 11 Comparison with the chemical production rates of Lee and Zierten[10] for *Re* = 814.

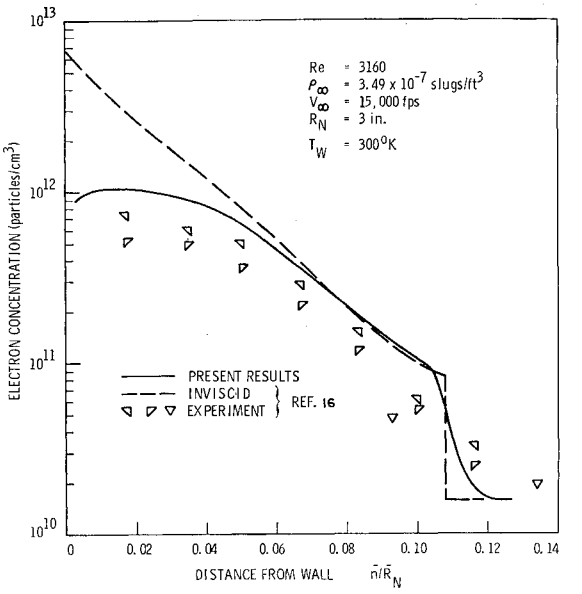

Fig. 12 Experimental and theoretical comparison of electron concentration.

change in the static enthalpy since it is proportional to the square of the normal velocity. For this case, the changes in the normal velocity are sufficient to cause the temperature differences observed in Fig. 10; hence, using the frozen flow static enthalpy to make the nonequilibrium calculations does not seem to be appropriate, at least in this case.

The present predictions for electron concentration have also been compared with experimental data. Figure 12 shows the results of such a comparison. The experimental data and the inviscid (streamtube) predictions shown in the figure were taken from Ref. 16. The presence of freestream electrons is due to the fact that the experimental data were obtained in a shock tunnel with a dissociated and ionized freestream. The present theoretical predictions allowed for this fact by using the appropriate species mass fraction values as freestream boundary conditions.

Good agreement is obtained between the experimental data and the merged layer prediction. Near the shock the inviscid and merged layer results are in close agreement; however, closer to the wall, a purely inviscid approach fails because no allowance is made for the important effects of wall cooling and diffusion.

The electron concentrations in Ref. 16 were obtained using a collisionless theory to interpret the probe measurements. However, the effects of collisions become more important near the wall where the density is increasing, and the probe characteristics are more likely to be described by a transition regime theory.[17] Taking into account the effects of collisions would tend to increase the experimental values of electron concentration shown in Fig. 12. Thus, a better agreement would be obtained between the data and the merged layer prediction. However, additional comparisons with other experimental results and a careful examination of the assumptions used in the merged layer analysis (such as constant *Le* = 1 and a simplified viscosity model) are needed in order to make final conclusions on the accuracy of the present model.

V. Conclusions

Nonequilibrium, multicomponent air calculations have been made for the stagnation merged layer of a hypersonic blunt body. Viscous and chemical relaxation effects are

taken into account in the entire region between the body surface and the freestream. Numerical solutions are obtained using a remarkably simple and rapid finite difference technique which allows the simultaneous calculation of the ionization and the detailed flowfield structure for a wide range of Reynolds numbers.

Some of the present results for the electron concentration have been compared with experimental data. It was found that the present predictions for the electron concentration are in good agreement with the experimental data throughout the merged layer. However, additional comparisons with experimental data are needed to establish the accuracy of the predicted electron concentrations for other conditions.

Comparisons have also been made with the predictions of two other theoretical models. The models are briefly, 1) an inviscid nonequilibrium theory and 2) an approximate merged layer analysis[10] in which the species conservation equations are uncoupled from the other fluid dynamic equations, and frozen flow properties are used to make the nonequilibrium calculation for the ionization. From the results of these comparisons, it was found that 1) an inviscid nonequilibrium theory overpredicts the merged layer ionization and 2) a coupled calculation, such as is used in the present investigation, should be used to compute the merged layer ionization.

References

[1] Probstein, R. F. and Kemp, N. H., "Viscous Aerodynamic Characteristics in Hypersonic Rarefied Gas Flow," *Journal of the Aerospace Sciences*, Vol. 27, No. 3, 1960, pp. 174–192.

[2] Ho, H. T. and Probstein, R. F., "The Compressible Viscous Layer in Rarefied Hypersonic Flow," *Rarefied Gas Dynamics*, edited by L. Talbot, Academic Press, New York, 1961, pp. 525–552.

[3] Chung, P. M., "Hypersonic Viscous Shock Layer of Nonequilibrium Dissociating Gas," Rept. TR R-108, 1961, NASA.

[4] Levinsky, E. S. and Yoshihara, H., "Rarefied Hypersonic Flow over a Sphere," *Hypersonic Flow Research*, edited by F. R. Ridell, Academic Press, New York, 1962, pp. 81–106.

[5] Goldberg, L. and Scala, S., "Mass Transfer in the Hypersonic Low Reynolds Number Viscous Layer," Rept. R62SD7, Jan. 1962, General Electric Co., Valley Forge, Pa.

[6] Cheng, H. K., "The Blunt-Body Problem in Hypersonic Flow at Low Reynolds Number," Rept. AF-1285-A-10, 1963, Cornell Aeronautical Lab., Buffalo, N.Y.

[7] Kao, H. C., "Hypersonic Viscous Flow Near the Stagnation Stream Line of a Blunt Body: I. A Test of Local Similarity," *AIAA Journal*, Vol. 2, No. 11, Nov. 1964, pp. 1892–1897.

[8] Edelman, R., "Nonequilibrium Hypersonic Air Flow in the Vicinity of the Stagnation Point," Rept. TR-449, Nov. 1964, General Applied Science Labs., Westbury, N.Y.

[9] Chung. P. M., Holt, J. F., and Liu, S. W., "Merged Stagnation Shock Layer of a Nonequilibrium Dissociating Gas," *AIAA Journal*, Vol. 6, No. 12, Dec. 1968, pp. 2372–2379.

[10] Lee, R. H. C. and Zierten, T. A., "Merged Layer Ionization in the Stagnation Region of a Blunt Body," *Proceedings of the 1967 Heat Transfer and Fluid Mechanics Institute*, Stanford University Press, Stanford, Calif., 1967, pp. 452–468.

[11] Hayes, W. D. and Probstein, R. F., *Hypersonic Flow Theory*, Academic Press, New York, 1959, p. 390.

[12] Holt, J. F., "Numerical Solution of Nonlinear Two-Point Boundary Problems by Finite Difference Methods," *Communications of the ACM*, Vol. 7, No. 6, June, 1964, pp. 366–373.

[13] Holt, J. F., "Numerical Solution of Nonlinear Two-Point Boundary Problems by Finite Differences Using Newton's Method," SAMSO-TR-68-385, May 1968, Aerospace Corp., San Bernardino, Calif.

[14] Strom, C. R., "Application of the Method of Nonlinear Simultaneous Displacements to General Three-Dimensional Stagnation Point Boundary Layer Equations," AIAA Paper 68-786, Los Angeles, Calif., 1968.

[15] Lew, H., "Method of Accelerated Successive Replacement Applied to Boundary Layer Equations," *AIAA Journal*, Vol. 6, No. 5, May 1968, pp. 929–931.

[16] Kaegi, E. M. and McMenamin, D. L., "Measured and Predicted Air Ionization in Blunt Body Shock Layers," AIAA Paper 69-81, New York, 1969.

[17] Talbot, L., "Langmuir Probe Characteristics in the Transition Regime," *Proceedings of the Sixth International Symposium on Rarefied Gas Dynamics*, MIT, Cambridge, Mass., July 22–26, 1968.